Connection between base drag, separating boundary layer characteristics and wake mean recirculation length of an axisymmetric blunt-based body

A. Mariotti[a,*], G. Buresti[a], M.V. Salvetti[a]

[a] *Dipartimento di Ingegneria Civile e Industriale, Università di Pisa, Via G. Caruso 8, 56122 Pisa, Italia*

Abstract

The variation of the base drag of an axisymmetric bluff body caused by modifications of the boundary-layer separating at the sharp-edged contour of its base is analysed through different numerical simulations, and the results are compared with those of a previous experimental investigation. Variational MultiScale Large-Eddy Simulations (VMS-LES) are first carried out on the same nominal geometry and at the same Reynolds number of the experiments. Subsequently, Direct Numerical Simulations (DNS) are performed at Reynolds numbers that are roughly two orders of magnitude lower, in order to investigate on the sensitivity of the main findings to the Reynolds number. The results of experiments, VMS-LES and DNS simulations show that an increase of the base pressure − and thus a decrease of the base drag − may be obtained by increasing the boundary layer thickness before separation, which causes a proportional increase of the length of the mean recirculation region

*Corresponding author

Email addresses: alessandro.mariotti@for.unipi.it (A. Mariotti), g.buresti@ing.unipi.it (G. Buresti), mv.salvetti@ing.unipi.it (M.V. Salvetti)

behind the body. In spite of the different set-ups, Reynolds numbers and turbulence levels in the experiments and numerical simulations, in all cases the base pressure is found to be directly proportional to the length of the mean recirculation region, which is thus a key index of the base drag value. In turn, the recirculation length seems to be connected with the location of the incipient instability of the detaching shear layers, which can be moved downstream by an increase of the thickness of the separating boundary layer and upstream by an increase of the turbulence level.
Keywords: Axisymmetric bodies, drag reduction, base drag, base pressure, wake recirculation

1. Introduction

The main contribution to the aerodynamic drag of a bluff body is normally given by the low pressures acting on its base, which is the part of the body surface lying within the separated wake. Decreasing the base drag would then have a considerable importance in many engineering applications, such as the design of low-consumption road vehicles. However, the present knowledge on the physical mechanisms influencing the base drag is still far from satisfactory; considerable research work is thus needed to reach a deep understanding of the physical mechanisms that influence the value of the pressures acting on the base of a bluff body and, consequently, to be able to devise methods to control it.

As a preliminary objective, it is of significant scientific interest to characterize the relationship between the base pressure and the parameters defining a particular flow configuration, and, especially, to identify the physical ori-

gin of this relationship. The present paper aims at giving a contribution in this direction, focusing, in particular, on the influence of the thickness of the boundary layer separating at the contour of the blunt base of an axisymmetric bluff body and trying to provide an explanation for the observed results. Indeed, some indications exist in the literature that the characteristics of the boundary layer developing over the lateral surface of a bluff body before its separation may influence the base pressure. This effect is particularly significant for bodies whose base is a sharp-edged flat surface perpendicular to the free stream. For instance, in the two-dimensional case the base drag of a thick plate with elliptic leading edge and flat base was found to decrease when the boundary-layer thickness was increased (see, e.g., Rowe et al., 2001). As for axisymmetric bodies in free air, some experimental data on the connection between separating boundary layer and base drag are available in the literature (see, e.g., Porteiro et al., 1983). However, to our knowledge the first experimental systematic investigation on this subject is documented in Mariotti and Buresti (2013), where the few relevant results available in the literature are also described in detail and an introductory discussion on the connection between base pressure and near wake flow features is reported. In the experiments of Mariotti and Buresti (2013) different thicknesses of the boundary layer developing over the lateral surface of an axisymmetric blunt-based body were obtained by adding small strips of emery cloth in various positions. The results showed that increasing the thickness of the boundary layer at separation – which was always turbulent – produced a reduction of the base suctions. Furthermore, a deeper analysis of the mean and fluctuating near wake flow suggested that this effect may be connected with an

increase of the length of the mean recirculation region present behind the body, which, in turn, is caused by a downstream movement of the incipient instability in the detaching shear layers.

In order to obtain further confirmation to the above experimental evidence, in the present paper we describe the results of numerical simulations carried out to widen the analysed flow conditions and to try to attain a deeper understanding of the parameters and flow features that are responsible for the ascertained connection between base pressure, boundary layer characteristics and near-wake flow features. Furthermore, considering that numerical simulations can also provide the complete flow dynamics, the obtained information is complementary to that given by the outputs of the experimental measurements, which were limited to hot-wire anemometry and pressure measurements over the body surface. A better description of the flow field is indeed important because it is known that the base pressure drag of bluff bodies is closely connected with the flow dynamics in the wake. For axisymmetric bodies this dynamics is more complex than the one characterizing two-dimensional bodies, which is dominated by the von-Karman vortex street. In particular, as the Reynolds number increases the wake undergoes several transitions associated with different wake regimes (see, e.g., Sevilla and Martinez-Bazan, 2004; Barkley, 2006; Bohorquez and Parras, 2011; Bohorquez et al., 2011; Bury and Jardin, 2012 for elongated axisymmetric bodies and Miau et al., 1997; Johnson and Patel, 1999; Mittal and Najjar, 1999; Kiya et al., 2001 for spheres and disks). Another advantage of numerical simulation is that the flow conditions are easier to be controlled than in experiments, and the effects of a given parameter may thus be sin-

gled out. However, to our knowledge no previous numerical investigations are available concerning the effect of the boundary layer thickness on the base drag and on the near-wake flow features of axisymmetric bodies. Some clues on the effect of the characteristics of the separating boundary layer on the near-wake velocity field and, in particular, on the length of the mean-flow recirculation region, may only be obtained from results on axisymmetric backward-facing steps (see, e.g., Hudy et al., 2005; Rajasekaran, 2011).

In this paper the variations of the base pressure obtained through boundary-layer and near-wake modifications are analysed by using two sets of numerical simulations, and the results are compared with the ones of the experimental investigation described in Mariotti and Buresti (2013). The objective of the simulations was not to exactly replicate the experiments but, rather, to ascertain whether the general trends found in the experimental campaign could be confirmed and explained also in significantly different flow conditions. First, Variational MultiScale Large-Eddy Simulations (VMS-LES) are carried out on the same nominal body geometry and at the same Reynolds number of the experiments. However, neither the wind tunnel free-stream turbulence nor the model support are present in the numerical simulations, and the variation of the boundary layer thickness is produced by using a free-slip boundary condition over different initial portions of the body surface. Subsequently, Direct Numerical Simulations (DNS) are performed at Reynolds numbers roughly two orders of magnitude lower than in the experiments and in the VMS-LES simulations, in order to investigate on the sensitivity of the relevant phenomena to the Reynolds number. In this case, only the flow over and downstream of the final portion of the axisymmetric body is simulated

and a self-similar laminar boundary-layer velocity profile with different thicknesses is imposed at the inlet of the computational domain. The comparison between all the various cases is carried out through the analysis of the mean base pressure and of the mean and fluctuating near-wake velocity field.

2. Problem definition and methodology

2.1. Experimental set up

The main features of the experimental set up of Mariotti and Buresti (2013) are now briefly recalled in order to highlight the differences with the numerical simulations. The tests were carried out in a closed-return, subsonic wind tunnel with a circular open test section $1.1m$ in diameter and $1.42m$ in length. The considered model is axisymmetric, has a forebody with a 3:1 elliptical contour and a cylindrical main body with a sharp-edged base perpendicular to the axis; its diameter to length ratio is $d/l = 0.175$. In the wind tunnel tests the body was supported above a flat plate by means of a faired strut (see Fig. 1(a)), where the adopted reference system is also shown). The chosen support implies that the flow is not symmetrical in the vertical plane, while it remains symmetrical in the horizontal plane; however, it was considered to be preferable than a rear sting support, which would interfere with the near-wake flow and change the free body base to an axisymmetric backward-facing step. The pressures over the body surface were obtained through a total of 121 pressure taps, 65 of which were distributed over the base, while the boundary layer profiles and the wake velocity field were characterized through hot-wire anemometry (see Mariotti and Buresti, 2013 for further details on the experimental apparatus and on the measurement tech-

niques). The tests were carried out at $Re = u_\infty d/\nu = 9.6 \times 10^4$, where u_∞ is the free-stream velocity. The wind tunnel free-stream turbulence intensity was 0.9%, and this caused the boundary layer over the lateral surface of the model to become turbulent before separating at the sharp-edged base contour, with an estimated transition located at approximately $x_t/l = -0.50$. In order to change the thickness of the boundary layer at separation, strips of emery cloth were wrapped in various positions around the body circumference in order to move transition upstream. In particular, the boundary layer transition was either kept natural or fixed at $x_t/l = -0.70$ and at $x_t/l = -0.875$ (see Figs. 1(b) and 1(c)).

2.2. Variational MultiScale Large Eddy Simulations

As already mentioned, the Variational MultiScale Large-Eddy Simulations are carried out on the same body and at the same Reynolds number of the wind tunnel tests. However, at variance with the experiments, laminar free-stream conditions are imposed and no model support is present (see Fig 2(a)). The method to change the boundary layer thickness is also different and exploits the possibility provided by numerical simulations of assuming non-physical flow conditions. Indeed, in the VMS-LES simulations a reduction of the boundary layer thickness, compared to the nominal situation for the considered Reynolds number, is obtained by using a free-slip boundary condition over different initial portions of the body lateral surface. In particular, three simulations are presented here, which correspond to no-slip over the entire body, over the last 75% and over the last 37.5% of the body length (see Figs. 2(b) and 2(c)).

The simulations were carried out by using AERO, an in-house developed

compressible flow solver. The numerical discretization is based on a linearized implicit time advancing and on a mixed finite-volume/finite-element method, applicable to unstructured grids. The accuracy of the numerical method is second order both in space and time.

The Smagorinsky subgrid scale model was used to close the VMS-LES equations. The code has been successfully used for the simulation of bluff-body flows in the past (see e.g. Camarri et al., 2004; Ouvrard et al., 2010; Wornom et al., 2011). The computational domain is cylindrical, with a diameter of $15d$ and a length of $50d$ ($30d$ being the distance from the body base to the outflow). This corresponds to a blockage factor of less than 0.5%. The domain size was chosen on the basis of the settings of previous LES simulations of bluff-body flows, carried out with the same code and the same boundary conditions (see, e.g., Ouvrard et al., 2010; Wornom et al., 2011), and on the sizes typically used in the literature for the numerical simulation of similar problems (see e.g. Bohorquez et al., 2011 and the references therein). Characteristic-based boundary conditions (see e.g. Camarri et al., 2004) are used at the inflow, outflow and lateral boundaries of the computational domain. At the inflow, a uniform and constant in time velocity is assumed such that the Reynolds number matches the one of the experiments. The free-stream Mach number is set equal to 0.1, so that compressibility effects are negligible. As previously explained, different boundary conditions are imposed on the body lateral surface in order to vary the boundary-layer thickness. Conversely, in all cases no-slip is imposed on the base of the body. An unstructured grid having approximately 2.4×10^6 nodes is used. The grid is particularly refined near the body surface, where the wall y^+ is lower

than 1, and in the near wake. Finally, the adopted dimensionless time step is $\Delta T = \Delta t(u_\infty/d) \cong 4.5 \times 10^{-3}$. This time step allowed us to have more than 1000 time steps in a shedding period of the hairpin vortices in the wake (see Section 2.3.2). Moreover, by defining the CFL number in each cell as CFL $= \Delta t(u/\Delta x)$, the adopted time step corresponds to a variable CFL, with a maximum value at each time step approximately equal to 2. This maximum CFL value is well below the stability limits of the adopted implicit time advancing scheme.

An overall impression of the results of the simulations and of the main flow features is provided by the longitudinal velocity and by the pressure coefficient for the case in which the no-slip condition is applied over the whole body surface; the relevant fields – averaged in time and in the azimuthal direction (see Section 3.1 for details) – are shown in Figs. 3(a) and 3(b), together with the mean flow streamlines. As can be seen, in the considered operating conditions the boundary layer remains completely attached over the lateral surface of the model up to the sharp-edged base contour. The subsequent flow separation leads to the development of a free shear layer and of a mean flow recirculation region behind the base, which ends with a trailing stagnation point. The outer mean-velocity streamlines bend aside this recirculation zone and, as will be explained in more detail in Section 3, their curvature is directly connected with the base drag.

2.3. Direct Numerical Simulations

2.3.1. Generalities on the numerical method

Direct Numerical Simulations were carried out only for the final portion of the previously described axisymmetric body. Thus, the considered geometry

comprises a cylindrical main body of length $s = 2d$ with a sharp-edged base perpendicular to the axis (see Fig. 4). The Reynolds number of the simulations is $Re_d = u_\infty d/\nu = 1500$.

Incompressible simulations were performed by using the open-source code OpenFOAM, which is based on the finite-volume discretization method (see e.g. OpenFOAM, 2009). Unsteady time advancing was chosen, together with an implicit scheme, and the pressure and momentum equations were coupled through the segregated PISO algorithm (see e.g. Issa, 1986). The accuracy of the numerical method is second order both in time and in space. The computational domain is cylindrical, with a diameter of $10d$ and a length of $30d$ ($28d$ being the distance from the body base to the outflow). The adopted domain size leads to a blockage factor of 1% and, as discussed previously in Section 2.2, it is in line with the domain dimensions adopted in similar numerical studies in the literature. A grid sensitivity study was carried out by using four hexahedral structured grids having approximately 1.4×10^6, 2×10^6, 3.5×10^6 and 5.3×10^6 nodes. Grid independence was evaluated on the mean values of the boundary layer characteristic thicknesses, viz. δ/d, δ^*/d, θ/d, of the pressure coefficient on the base of the body, Cp_{base}, and of the mean recirculation length, l_r. The convergence was considered to be reached when all the above quantities differed by less than 0.5%; this criterion was satisfied by the grid having approximately 3.5×10^6 nodes, which was then used for the subsequent simulations. The grid is obtained by using 7.2×10^4 nodes in the diametral planes and 48 nodes in the azimuthal direction. The adopted dimensionless time step is $\Delta T = \Delta t(u_\infty/d) = 7 \times 10^{-3}$, leading to about 1000 time steps in a shedding period of the hairpin vortices. Moreover,

the adopted time step corresponds to a variable CFL number, whose average value in the computational domain is approximately 0.3 with maximum peaks up to 2.5. These CFL values are well below the stability limits of the adopted implicit time advancing scheme.

The method to change the boundary layer thickness is again different from the ones of the experiments and of the VMS-LES simulations. Indeed, an axisymmetric self-similar laminar boundary-layer velocity profile is directly assumed at the inlet of the computational domain, with three different values of the thickness δ_{in}/d, viz. $\delta_{in}/d = 0.1$, $\delta_{in}/d = 0.2$, and $\delta_{in}/d = 0.3$. This set up permits to obtain, over the final part of the body, boundary layer thicknesses that are comparable to those found in the experiments and in the VMS-LES simulations, in spite of the much lower Reynolds number. Clearly, this would not have been possible by considering the natural evolution of the boundary layer over the whole body. As was checked a posteriori, the length of the simulated body portion, $s = 2d$, is sufficient to avoid spurious pressure perturbations caused by the inlet conditions on the last portion of the body surface ($1.5d$ long). Furthermore, the start of the pressure variation on the lateral surface occurs only in the last diameter from the base contour, similarly to what happened in the experiments (see Mariotti and Buresti, 2013). The verification of the self-similarity of the boundary-layer velocity profiles for a sufficiently-long circular cylinder in axial flow is reported in Mariotti (2014). No-slip is imposed on the body while free slip is used on the domain lateral boundary, together with pressure outflow conditions.

2.3.2. Validation of the DNS computational set up

In order to verify that the simulation of the last part of the body shown

in Fig. 4 , with the previously described inlet conditions, provides results that are adequate to represent the flow field downstream of an axisymmetric elongated body with attached boundary layer up to its base contour, a preliminary activity was conducted to validate the computational set up. In particular, a comparison was carried out against results available in the literature for the same type of bodies at low Reynolds numbers (see e.g. Bohorquez and Parras, 2011; Bohorquez et al., 2011; Bury and Jardin, 2012). To this aim, three simulations were carried out for three different Reynolds numbers, viz. $Re_d = 300, 800$ and 1500, which are representative of the three characteristic flow regimes that can be found downstream of such bodies at low Reynolds numbers. For $Re_d \leq 460$ the velocity field downstream of the body is characterized by a stationary axisymmetric recirculation region. Conversely, in the range $460 \leq Re \leq 910$ the flow shows an unsteady planar-symmetric solution. As the Reynolds number increases above a second threshold, i.e. for $Re_d \geq 910$, a second instability is found in the form of a three-dimensional peristaltic oscillation modulating the vortices, which eventually leads to the shedding of hairpin vortices.

The three Direct Numerical Simulations have been able to well capture the previously described flow patterns. In particular, at $Re_d = 300$ the stationary axisymmetric recirculation characterizing the flow was recovered; this can be seen in Fig. 5, where the instantaneous streamlines are reported together with the x-velocity. Note that in Fig. 5 the results for the plane $z/d = 0$ are shown, but, since the solution is axisymmetric, they can be considered as representative of any generic streamwise plane in the near wake. For the simulation at $Re_d = 800$ the recirculation region is no more axisymmetric and

a planar symmetry is found, with two different couples of principal planes in the near and in the far wake, respectively denoted as $y'/d = 0 - z'/d = 0$ and $y''/d = 0 - z''/d = 0$. The angular separation between the two couples of principal planes was found to be approximately 45°, as in Bohorquez and Parras (2011). As for the near wake, from the visualization of the streamlines in the principal planes $z'/d = 0$ and $y'/d = 0$ (see Fig. 6(a) and Fig. 6(b)) it is evident that two counter-rotating steady recirculations are found in the plane $z'/d = 0$, while an oscillatory dynamics is present in the plane $y'/d = 0$. Indeed, the pattern of Fig. 6(b) changes to an opposite one − i.e. the one that is obtained from a rotation of 180° around the x-axis − after half period of the shedding of hairpin vortices that occurs more downstream. This shedding is evident in Fig. 7, where instantaneous isosurfaces of the vortex-indicator λ_2 (see e.g. Jeong and Hussain, 1995; Chakraborty et al., 2005) are reported. The Strouhal number of the vortex shedding was found to be $St \cong 0.13$, which is similar to the Strouhal value obtained by Bohorquez et al. (2011).

The unsteady flow deriving from the DNS at $Re_d = 1500$ is again characterized by the formation and evolution of hairpin vortices (see e.g. Sevilla and Martinez-Bazan, 2004; Barkley, 2006; Bohorquez and Parras, 2011; Bohorquez et al., 2011; Bury and Jardin, 2012), as can be qualitatively seen, for instance, from the instantaneous isosurfaces of the vortex-indicator λ_2 shown in Fig. 8. However, from the dynamic visualization of the wake flow field (not shown here for the sake of brevity) it could be observed that, at variance with the previous regime, in this case the symmetry plane of the shedding continuously rotates in time, as already found, for instance, by Grandemange

et al. (2012).

3. Comparative analysis of the results

The DNS results obtained at $Re = 1500$ are compared here with the LES ones as well as with the experimental findings in Mariotti and Buresti (2013).

3.1. Mean quantities

All the flow statistics were computed by neglecting an initial numerical transient and then using a time length equal to $T = tu_\infty/d = 60$ for the DNS and to $T = 55$ for the VMS-LES. Furthermore, the quantities indicated as "mean" in the following are obtained by averaging both in time and in the azimuthal direction. As was shown in Section 2.3.2, in the considered cases the wake dynamics is characterized by vortical structures shedding on planes continuously rotating in time; the statistics may be reasonably assumed to be homogeneous in the azimuthal direction. The averaging time windows have been chosen on the basis of an analysis of the statistical convergence of the mean values of the boundary layer characteristic thicknesses, viz. δ/d, δ^*/d, θ/d, of the pressure coefficient on the base of the body, Cp_{base}, and of the mean recirculation length, l_r. By comparing the mean values of all these quantities computed over the above mentioned time intervals and over approximately 25% shorter ones, it was found that they differed by less than 1% for LES and by less than 0.5% for DNS (see Mariotti, 2014 for the convergence analysis of the mean statistics).

The mean values of the boundary layer thickness, δ/d, at $x/d = -0.1$ obtained in the experiments of Mariotti and Buresti (2013) and in the two types of numerical simulations are reported in Table 1, where the corresponding

mean values of the displacement thickness δ^*/d, of the momentum thickness θ/d and of the shape factor H are also given. As the considered position lies within a region where a negative pressure gradient along the surface is present, with a consequent accelerating velocity at the edge of the boundary layer (see Fig. 7 in Mariotti and Buresti, 2013), the values of δ/d are obtained by identifying the distance normal to the surface at which the mean velocity is equal to 99% of the maximum one in the considered section. Within numerical uncertainty, this position coincides with the one corresponding to 99% of the integral of the vorticity in the normal direction. As can be seen, the whole set of cases comprises a wide range of boundary layer thicknesses; furthermore, the values of the shape factor witness that in the experiments all boundary layers were turbulent at separation, whereas they are laminar or in incipient transition for the DNS and VMS-LES simulations. These differences are consistent with the laminar free-stream conditions and, in the DNS case, also with the lower Reynolds number.

As already pointed out, in all the considered operating conditions the boundary layer remains completely attached over the lateral surface of the model up to the separation at the sharp-edged base contour, which leads to the development of a free shear layer in the near wake and to a flow recirculation ending at a trailing stagnation point. Therefore, the streamlines bounding the recirculation zone have a curvature that is first convex and then concave; this leads first to a decrease and then to an increase in pressure, which are respectively connected with an increase and a decrease in velocity. This trend was indeed observed in the experiments of Mariotti and Buresti (2013) (see, in particular, Fig. 7) and it was confirmed by the

Methodology	Case	δ/d	δ^*/d	θ/d	H
Experiments	Smooth model	0.107	0.0121	0.0086	1.41
	One strip of emery cloth	0.143	0.0171	0.0121	1.41
	Two strips of emery cloth	0.171	0.0194	0.0144	1.35
VMS-LES	No-slip over 37.5% of the body	0.0306	0.0078	0.0036	2.15
	No-slip over 75% of the body	0.0411	0.0107	0.0050	2.14
	No-slip over the entire body	0.0663	0.0146	0.0072	2.03
DNS	$\delta_{in}/d = 0.1$	0.171	0.0539	0.0232	2.32
	$\delta_{in}/d = 0.2$	0.234	0.0739	0.0321	2.30
	$\delta_{in}/d = 0.3$	0.318	0.1024	0.0441	2.32

Table 1: Boundary layer characteristics evaluated at $x/d = -0.1$

present simulations (not shown here for the sake of brevity). As observed in Mariotti and Buresti (2013), the value of the velocity outside the separating boundary layer and along the first part of the free shear layer bounding the recirculation region is directly linked to the value of the pressure on the body base. The effect of increasing the boundary layer thickness on the shape and dimension of the recirculation region may be appreciated from Fig. 9(a) and Fig. 9(b), which show, respectively for the VMS-LES and the DNS simulations, the mean flow streamlines bounding the recirculation region, together with the wake edges, evaluated as the positions corresponding to 99% of the integral of the vorticity in the cross-flow direction. As already found in the experiments, increasing the boundary layer thickness leads to an increase of the recirculation length l_r/d, which may be determined from the position along the wake axis were the mean velocity value is equal to zero. As a

consequence, the curvature of the streamlines bounding the first part of the recirculation region decreases, causing an analogous reduction of the velocity. As can be seen from the mean pressure distributions reported, for the two types of simulation, in Fig. 10(a) and Fig. 10(b), the result is an increase of the mean base pressure − and, thus, a reduction of the base drag − with increasing thickness of the separating boundary layer.

The experimental base pressure measurements described in Mariotti and Buresti (2013) were obtained only for radial distances $r \leq 0.4$. Therefore, in order to directly compare the effects of the boundary layer thickness on the base drag obtained in the experiments and in the two types of numerical simulations, the numerical mean pressure coefficients were averaged over this limited portion of the base, and the corresponding values are denoted as $Cp_{base}^{r\leq 0.4}$. The complete set of values obtained for this parameter is reported as a function of the boundary layer thickness in Fig. 11(a). From this figure one may immediately observe that for all the considered cases $Cp_{base}^{r\leq 0.4}$ increases almost linearly with increasing δ/d. However, significant quantitative differences are found between the experiments and the present numerical methods; in particular, it is apparent that comparable values of the boundary layer thickness may give rise to quite different base pressures. This result may be readily explained by considering the different conditions corresponding to the various cases, and by analyzing the variations of the recirculation length as a function of the boundary layer thickness, which are shown in Fig. 11(b). Note that the values of l_r/d could not be accurately measured in the experiments of Mariotti and Buresti (2013), but they could be inferred from the positions corresponding to maximum fluctuations in the

axis, as described in Mariotti (2014). Figure 11(b) shows that the trends of l_r/d as a function of δ/d are similar to those of $Cp_{base}^{r\leq 0.4}$. For instance, low experimental base pressures − and thus high drags − in Fig. 11(a) correspond to low values of l_r/d in Fig. 11(b). Analogous differences between the experimental and numerical results are also found. The reasons of these quantitative difference will be analysed in more detail in the following.

The similarity of the trends in Figs. 11(a) and 11(b) immediately suggests the existence of a direct connection between the mean base pressure and the recirculation length, and this is what derives from Fig. 12, where $Cp_{base}^{r\leq 0.4}$ is reported as a function of l_r/d. Indeed, all the experimental and numerical data of the base pressure are seen to follow a common and almost linear relationship with the recirculation length. This result strongly indicates that, independently of the status of the boundary layer before separation, of the turbulence level of the oncoming flow and of the Reynolds number, the mean recirculation length is directly correlated with the base pressure, and thus with the base drag. In particular, the base suctions and drag decrease with increasing l_r/d. In other words, the present results suggest that the mean recirculation length may be assumed as a direct index of the base drag of an axisymmetric body and, thus, a possible parameter to be controlled in order to modify the base drag.

3.2. Analysis of the near wake

The above-described findings suggest the need of carrying out a deeper investigation on the physical mechanisms that influence the length of the recirculation region, and a significant clue in this direction is provided by the analysis of the fluctuating flow field. Indeed, the mean flow features in the

near wake are the result of the instantaneous flow dynamics. In all cases, the wake is found to be characterized by the formation and evolution of hairpin vortices, as schematically depicted in Fig. 13, in agreement with the results obtained on similar bodies and on spheres at low Reynolds numbers. In this general framework, differences are again observed between the results of the experiments and of the numerical simulations. In the latter, these vortical structures form and evolve on planes rotating with time but, due to the higher Reynolds number, their formation occurs more upstream in the VMS-LES simulations than in DNS ones. The different qualitative evolution of the structures can be inferred, for instance, by comparing Fig. 14 with Fig. 8, where isosurfaces of the vortex-indicator λ_2 are respectively shown for the VMS-LES with no-slip condition over the whole body and for the DNS simulation. In the experiments of Mariotti and Buresti (2013), the hairpin vortices had been found to form only on a preferential fixed plane due to the presence of the faired support.

The connection between the mean and fluctuating flow fields, in spite of the different and complex wake dynamics characterizing the various cases, may be explained by considering the different locations where the instability of the shear layers bounding the near-wake occurs. As already suggested in Mariotti and Buresti (2013), this location may be identified by analysing the trends of the standard deviation of the velocity fluctuations along the edge of the near-wake, which are shown, for all the different experimental and numerical cases, in Figs. 15(a), 15(b) and 15(c). As may be seen, the fluctuations start increasing at a certain distance from the base which, in all cases, increases with increasing boundary layer thickness. Furthermore, the

increase occurs progressively more downstream going from the experimental results to those of the VMS-LES and of the DNS simulations, in agreement with the increasing values of l_r/d for the various cases shown in Fig. 11(b). Therefore, it is plausible to deduce that this growth of the velocity fluctuations be associated with the onset of an instability in the separated shear layer bounding the near wake and that, in turn, the length of the mean recirculation region be determined by the location of this instability.

The above result is thus consistent with the fact that l_r/d may indeed be expected to be dependent on all the flow features which may cause the shear layer to become unstable. For instance, the instability onset should move upstream when the turbulence level within the separating shear layer and in the free-stream increases and this explains the significantly lower values of the recirculation lengths that were found in the experiments as a function of the boundary layer thickness (see Fig. 11(b)). Furthermore, for a given value of δ/d and of the turbulence level, a higher velocity value outside the boundary layer at separation would give rise to a following shear layer with a velocity profile having a higher gradient at its inflection point, and this should promote a more rapid instability. Although some effects of discretization and modelling errors cannot be excluded in the VMS-LES simulations, this observation provides a possible explanation for the quantitative differences that may also be observed in Fig. 11(b) between the trends of the recirculation length corresponding to the VMS-LES and the DNS simulations. Indeed, although in that figure no values deriving from the two types of simulation are reported for the same values of the boundary layer thickness, the two linear relationships that may represent the relevant data seem

to be vertically displaced. In other words, if the straight line corresponding to the DNS data were continued towards lower values of δ/d, the DNS simulations would produce slightly shorter recirculation lengths than the VMS-LES ones for hypothetical coincident values of δ/d. In this case the fundamental feature distinguishing the two numerical simulations is probably the different boundary layer development before separation. Indeed, even assuming in both cases laminar flow to be present, the Reynolds numbers differ by almost two orders of magnitude. Furthermore, the boundary layer imposed as an input for the DNS simulations corresponds to an imaginary cylindrical axisymmetric body of appropriate length, whereas the VMS-LES simulations were carried out for the same body used in the experiments, with the consequent presence of positive and negative pressure gradients over the forebody and the first part of the cylindrical main body. Therefore, the evolution of the boundary layer thickness along the last portion of the body lateral surface is significantly different in the two cases, as may be appreciated in Fig. 16, where the results of a DNS and a VMS-LES simulation are compared. In particular, due to the above mentioned differences, a higher rate of increase of δ/d before separation is found, as expected, for the lower-Reynolds DNS simulations. It is then reasonable to infer that, for comparable values of the boundary layer thickness at separation, the outer velocity would be higher in the low-Reynolds case.

3.3. Further discussion on the results

One might wonder why, in a situation in which the near-wake flow is clearly unsteady and apparently dominated by the dynamics of different vorticity structures, should it be possible to derive an important index related

to the mean base drag from the mean velocity field, which actually never coincides with the continuously varying instantaneous flow field. A possible explanation derives from the observation that all the available experimental and numerical results confirm that the base pressure of a bluff body is either equal or closely connected with the pressure acting at the point of separation of the boundary layer on the base contour. Consequently, a direct link exists between the base pressure and the square of the value of the velocity outside the separating boundary layer. However, even if downstream of the recirculation region the velocity fluctuations may significantly increase due to the shedding of vorticity structures, the square of the ratio between the velocity fluctuations and the mean velocity in the region outside the separating boundary layer is usually not large, and this may explain why the mean base pressure is mainly dependent on the mean velocity field. This should be particularly true for axisymmetric bodies, for which the shed vortical structures are definitely weaker and less organized than happens for two-dimensional bodies with a regular shedding of strong and concentrated vortices. Considering that the mean velocity outside the separating boundary layer is an increasing function of the convex curvature of the mean streamlines bounding the initial part of the recirculation region, the consequence of the above is that the shorter is the recirculation length the higher one may expect to be the outer mean velocity at separation and the base drag.

A closer analysis of the results reported in Fig. 9 and in Fig. 12 permits also to appreciate that the variations of the base drag that derive from small changes in the shape of the initial part of the boundary of the recirculation regions may be very large indeed. This is not really surprising because it

is a well-known feature of the flow around aerodynamic bodies with thin and attached boundary layers that in a potential flow small variations of the curvature of the streamlines may produce large variations of the velocity and pressure fields. The present investigation shows that in certain cases the analysis of the behaviour of the outer potential flow may also be useful to explain the trends of data relating to bluff bodies with large separated wakes. It must also be pointed out that the significant influence of the separating boundary layer characteristics – which may be affected by a large number of flow field and geometrical parameters – may justify, at least in part, the scatter that is often found in the experimental and numerical data for the drag of bluff bodies.

4. Conclusions

The effect of varying the boundary layer thickness on the lateral surface of an axisymmetric blunt-based body was analysed through VMS-LES and DNS simulations, and the results were compared with available experimental data. The experiments and the VMS-LES simulations were carried out at the same Reynolds number but the free stream and boundary layer turbulence levels were different. On the other hand, the DNS simulations were performed at a significantly lower value of the Reynolds number. The results show that in all cases the base drag of the body decreases when the thickness of the separating boundary layer increases. The trend of this variation is the same for all the considered cases but significant quantitative differences are present, which are consistent with the different flow conditions as regards turbulence level and Reynolds number. However, considering the effect of

the variation of the boundary layer thickness on the length of the mean recirculation region present in the near wake, it could be ascertained that, independently of the status of the boundary layer before separation, of the turbulence level of the incoming flow and of the Reynolds number, a single approximately-linear relationship exists between the base pressure and the mean recirculation length, which is thus identified as a key index of the value of the base drag. This highlights the importance of identifying the main flow parameters and features that influence the mean recirculation length.

In the present work we initially focused on the effect of the thickness of the separating boundary layer, but a closer analysis of the comparison between the results of the experiments and of the different numerical simulations permitted to highlight the importance of the near-wake dynamics. Indeed, it was shown that a fundamental role is played by the behaviour of the velocity fluctuations in the shear layer bounding the near wake and, in particular, by the location where they significantly increase. In turn, this location is dependent on various other flow features besides the thickness of the separating boundary layer, such as the turbulence level inside and outside it. Furthermore, for the same boundary layer thickness and turbulence level, one may have different values of the external velocity according to the previous development of the boundary layer, which is connected with the shape of the forebody and with the Reynolds number. Although they have not been systematically investigated herein, all these different effects were shown to be present in the results of our investigation, but were also found not to affect the relation between base drag and mean recirculation length.

Finally, the direct correlation that was shown to exist between the length

of the mean recirculation region and the base drag of axisymmetric bluff bodies should not be interpreted as a cause-effect relationship. In other words, what has been verified is only that a high base drag corresponds to a short recirculation length. This finding may be explained by recalling that the drag acting on a body moving in an otherwise still fluid is connected with the continuous supply of kinetic and internal energies to the fluid. This perturbation energy is an increasing function of the amounts of vorticities of opposite sign introduced into the wake in unit time, of their distance and of their degree of concentration in restricted regions (see, e.g., Buresti, 2012). Alternatively, the drag may be expressed in terms of the time variation of the axial moment of vorticity, which is again essentially connected with the vorticity being continuously introduced in the wake downstream of the recirculation region (see, e.g., Wu et al., 2006). Therefore, a large mean drag is associated with strong and concentrated vorticity structures in the wake, whose effect is to induce high upstream-directed velocities, thus generating a short mean recirculation length. In practice, all the flow features that cause a high drag to act on a moving bluff body also contribute to the formation of a short mean recirculation length.

In any case, the ascertained correlation between base drag and recirculation length may also have a significant practical importance. For instance, it suggests that any geometrical or flow modification influencing the value of the recirculation length may also be expected to affect the base drag. Therefore, when developing optimization procedures aimed at reducing the drag of blunt-based bluff bodies, the objective function might be expressed in terms of the recirculation length. The interest of this alternative choice

derives from the fact that, in certain cases, the identification of the end of the recirculation region may be computationally advantageous compared to the direct evaluation of the base drag.

Acknowledgments

The authors wish to thank Nicola Pineschi, Fabio Macaddino and Stefano D'Andrea for their precious contribution in carrying out the numerical simulations. The Italian computing centre CINECA is gratefully acknowledged for providing computational resources.

References

Barkley, D., 2006. Linear analysis of the cylinder wake mean flow. Europhys. Lett. 75 (5), 750–756.

Bohorquez, P., Parras, L., 2011. Three-dimensional numerical simulation of the wake flow of an afterbody at subsonic speeds. Theor. Comput. Fluid Dyn. 27 (1-2), 201–218.

Bohorquez, P., Sanmiguel-Rojas, E., Sevilla, A., Jiménez-González, J., Martínez-Bazán, C., 2011. Stability and dynamics of the laminar wake past a slender blunt-based axisymmetric body. J. Fluid Mech. 676, 110–144.

Buresti, G., 2012. Elements of Fluid Dynamics. Imperial College Press, London.

Bury, Y., Jardin, T., 2012. Transitions to chaos in the wake of an axisymmetric bluff body. Physics Lett. 376, 3219–3222.

Camarri, S., Salvetti, M. V., Koobus, B., Dervieux, A., 2004. A low-diffusion muscl scheme for les on unstructured grids. Comp. Fluids 33, 1101–1129.

Chakraborty, P., Balachandar, S., Adrian, R. J., 2005. On the relationships between local vortex identification schemes. J. Fluid Mech. 535, 189–214.

Grandemange, M., Gohlke, M., Parezanovic, V., Cadot, O., 2012. On experimental sensitivity analysis of the turbulent wake from an axisymmetric blunt trailing edge. Phys. Fluids 24: 035106.

Hudy, L. M., Naguib, A. M., Humphreys, W. M., Bartram, S. M., 2005. Particle image velocimetry measurements of a two/three-dimensional separating/reattaching boundary layer downstream of an axisymmetric backward-facing step. 43rd AIAA Aerospace Sciences Meeting and Exhibit, AIAA Paper 2005-0114.

Issa, R. I., 1986. Solution of the implicit discretized fluid flow equations by operator splitting. J. Comput. Phys. 65 (1), 40–65.

Jeong, J., Hussain, F., 1995. On the identification of a vortex. J. Fluid Mech. 285, 69–94.

Johnson, T. A., Patel, V. C., 1999. Flow past a sphere up to a Reynolds number of 300. J. Fluid Mech. 378, 19–70.

Kiya, M., Ishikawa, H., Sakamoto, H., 2001. Near-wake instabilities and vortex structures of three-dimensional bluff bodies: a review. J. Wind Eng. Ind. Aerod. 89, 1219–1232.

Mariotti, A., 2014. Experimental and numerical investigations for the characterization and control of separated flows. Ph.D. Thesis, Scuola di Dottorato in Ingegneria "Leonardo da Vinci", University of Pisa.

Mariotti, A., Buresti, G., 2013. Experimental investigation on the influence of boundary layer thickness on the base pressure and near-wake flow features of an axisymmetric blunt-based body. Exp. Fluids 54 (11): 1612.

Miau, J. J., Leu, T. S., Liu, T. W., Chou, J. H., 1997. On vortex shedding behind a circular disk. Exp. Fluids 23, 225–233.

Mittal, R., Najjar, F., 1999. Vortex dynamics in the sphere wake. AIAA J. 99, 3806–3814.

OpenFOAM, 2009. Openfoam 1.6 user's guide. www.openfoam.org.

Ouvrard, H., Koobus, B., Dervieux, A., Salvetti, M., 2010. Classical and variational multiscale LES of the flow around a circular cylinder on unstructured grids. Comp. Fluids 39, 1083–1094.

Porteiro, J. L. F., Przirembel, C. E. G., Page, R. H., 1983. Modification of subsonic wakes using boundary layer and base mass transfer. AIAA J. 21, 665–670.

Rajasekaran, J., 2011. On the flow characteristics behind a backward-facing step and the design of a new axisymmetric model for their study. Master of Applied Science Thesis, University of Toronto.

Rowe, A., Fry, A. L. A., Motallebi, F., 2001. Influence of boundary-layer

thickness on base pressure and vortex shedding frequency. AIAA J. 39, 754–756.

Sevilla, A., Martinez-Bazan, C., 2004. Vortex shedding in high Reynolds number axisymmetric bluff-body wakes: Local linear instability and global bleed control. Phys. Fluids 16, 3460–3469.

Wornom, S., Ouvrard, H., Salvetti, M., Koobus, B., Dervieux, A., 2011. Variational multiscale large-eddy simulations of the flow past a circular cylinder: Reynolds number effects. Comp. Fluids 47, 47–50.

Wu, J. Z., Ma, H. Y., Zhou, M. D., 2006. Vorticity and vortex dynamics. Springer.

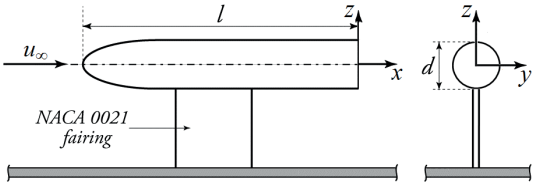

(a) Geometry, main parameters and reference system

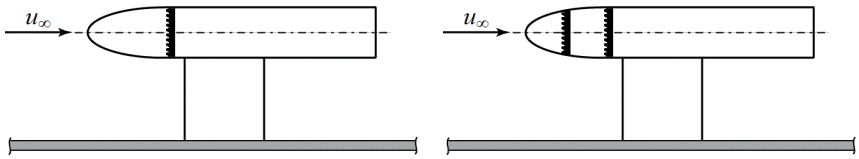

(b) Model with one strip of emery cloth

(c) Model with two strips of emery cloth

Figure 1: Sketch of the experimental set up

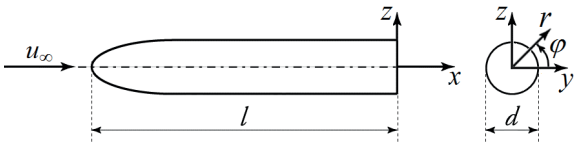

(a) Geometry, main parameters and reference system

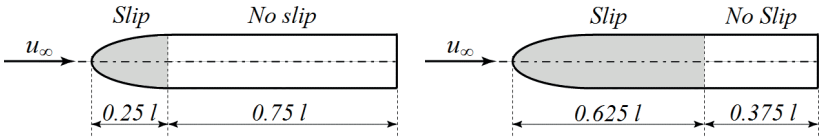

(b) No-slip over 75% of the body

(c) No-slip over 37.5% of the body

Figure 2: Sketch of the VMS-LES set up

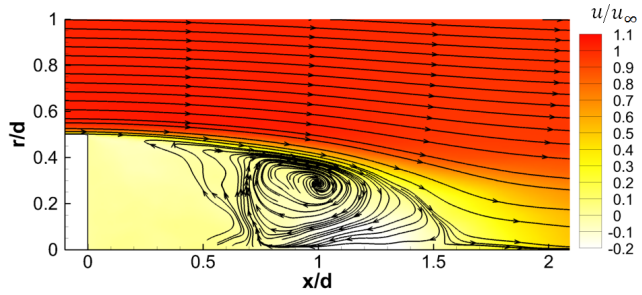

(a) x-velocity field

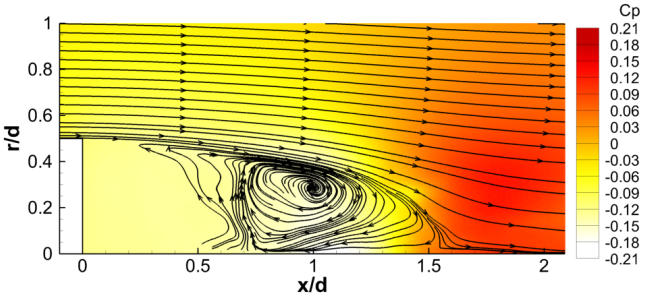

(b) Pressure coefficient field

Figure 3: Streamlines of the velocity field averaged in time and in the azimuthal direction

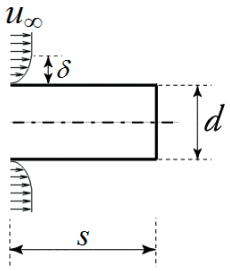

Figure 4: Sketch of the DNS set up

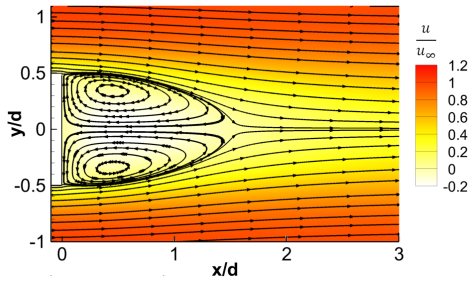

Figure 5: Streamlines downstream of the body at $Re_d = 300$

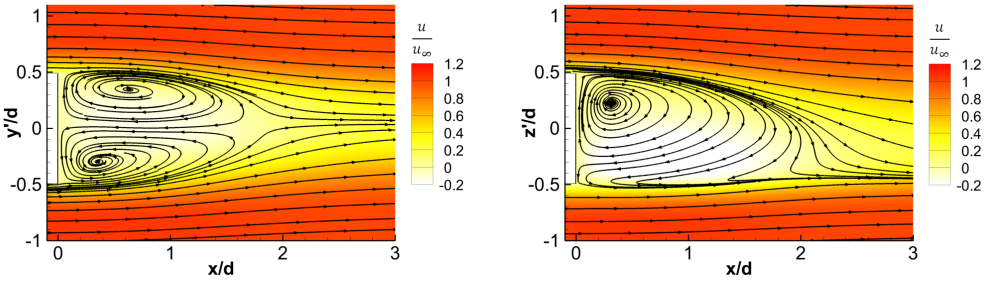

(a) Plane $z'/d = 0$ (b) Plane $y'/d = 0$

Figure 6: Streamlines downstream of the body in the principal planes at $Re_d = 800$

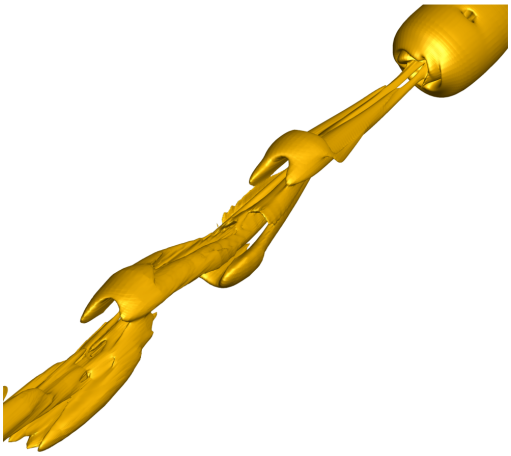

Figure 7: Isosurfaces of the vortex-indicator λ_2 at $Re_d = 800$

Figure 8: Isosurfaces of the vortex-indicator λ_2 at $Re_d = 1500$

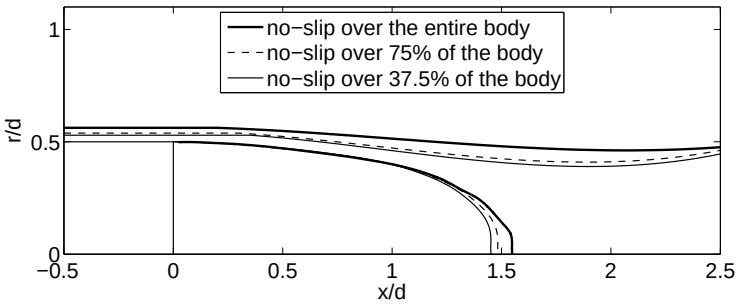

(a) VMS-LES

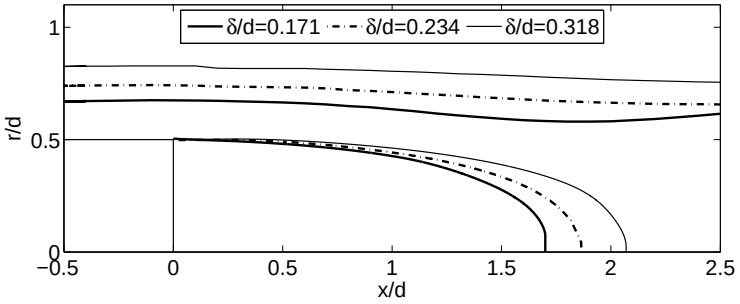

(b) DNS

Figure 9: Mean flow streamlines bounding the recirculation zone and wake edges

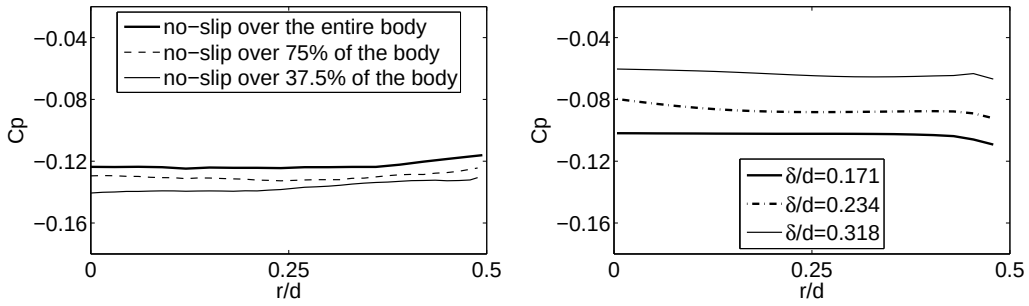

(a) VMS-LES (b) DNS

Figure 10: Variation of the mean Cp over the base

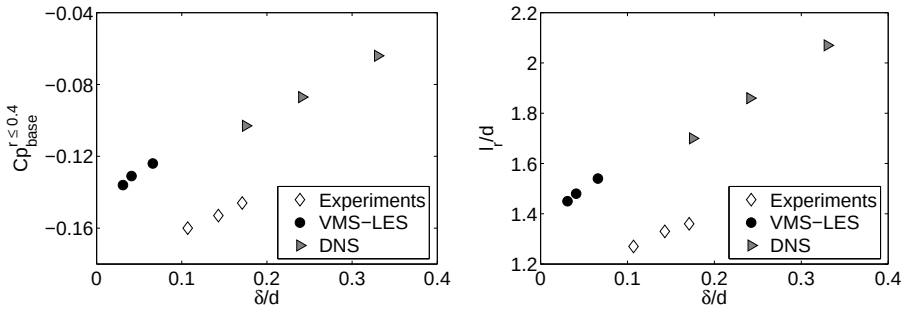

(a) $Cp_{base}^{r\leq 0.4}$ vs. δ/d (b) l_r/d vs. δ/d

Figure 11: Comparison between the experimental, the VMS-LES and the DNS results

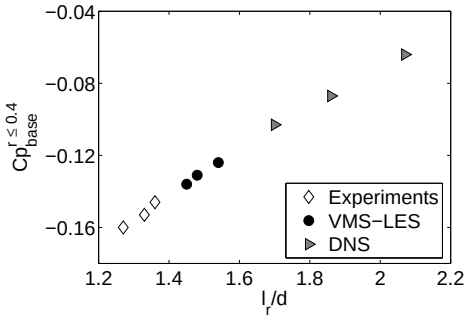

Figure 12: Comparison between the experimental, the VMS-LES and the DNS results: $Cp_{base}^{r\leq 0.4}$ vs. l_r/d.

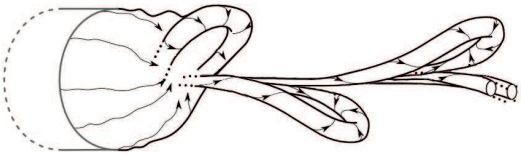

(a) Time $t = t^*$

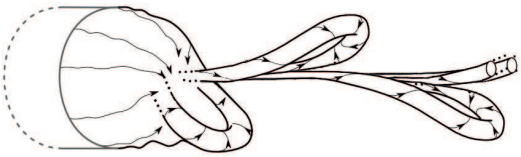

(b) Time $t = t^* + \frac{1}{2}T$

Figure 13: Sketch of the hairpin vortices downstream of the axisymmetric body

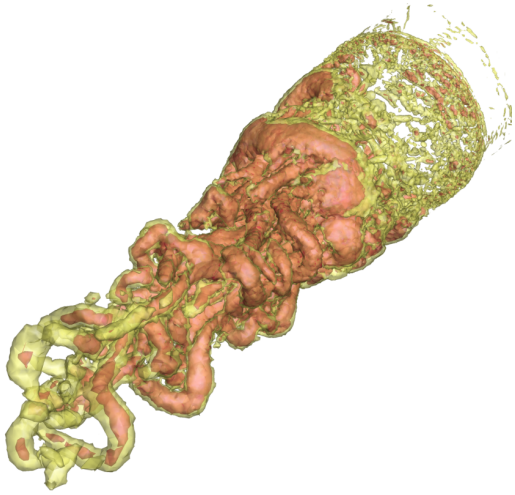

Figure 14: Isosurfaces of the vortex-indicator λ_2 for VMS-LES with no-slip condition over the whole body

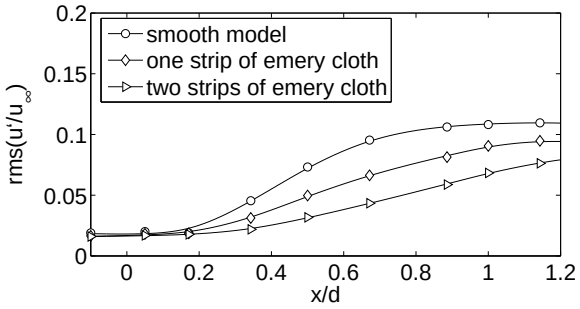

(a) Experiments

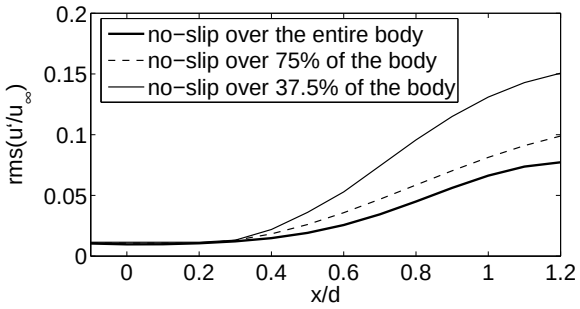

(b) VMS-LES

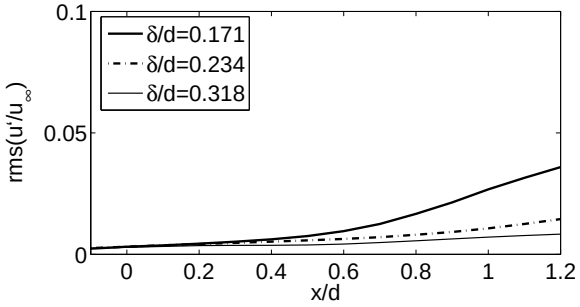

(c) DNS

Figure 15: Values of the rms of x-velocity fluctuations along the edges of the boundary layer and of the near wake

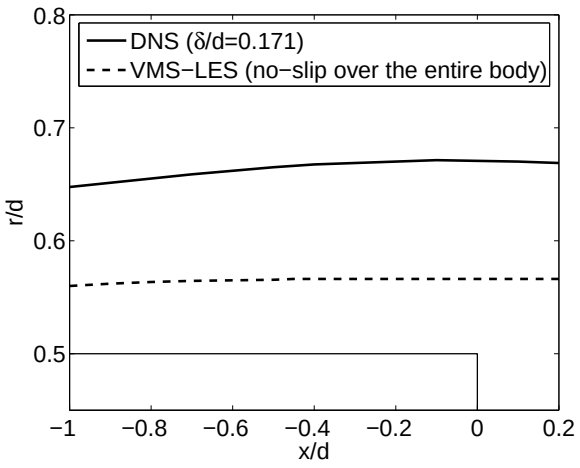

Figure 16: Evolution of the boundary layer thickness along the last portion of the body for the VMS-LES and the DNS